

Have greenhouse gases intensified the contrast between wet and dry regions?

Article

Accepted Version

Main text of the article and supplementary information

Polson, D., Hegerl, G. C., Allan, R. and Balan Sarojini, B. (2013) Have greenhouse gases intensified the contrast between wet and dry regions? *Geophysical Research Letters*, 40 (17). pp. 4783-4787. ISSN 0094-8276 doi: <https://doi.org/10.1002/grl.50923> Available at <http://centaur.reading.ac.uk/34442/>

It is advisable to refer to the publisher's version if you intend to cite from the work. See [Guidance on citing](#).

Published version at: <http://dx.doi.org/10.1002/grl.50923>

To link to this article DOI: <http://dx.doi.org/10.1002/grl.50923>

Publisher: American Geophysical Union

All outputs in CentAUR are protected by Intellectual Property Rights law, including copyright law. Copyright and IPR is retained by the creators or other copyright holders. Terms and conditions for use of this material are defined in the [End User Agreement](#).

www.reading.ac.uk/centaur

CentAUR

Central Archive at the University of Reading

Reading's research outputs online

¹ Have greenhouse gases intensified the contrast ² between wet and dry regions?

D. Polson,¹ G.C. Hegerl,¹ R. P. Allan,², and B. Balan Sarojini,³

¹School of GeoSciences, Grant Institute,
The University of Edinburgh, The King's
Buildings, West Mains Road, Edinburgh
EH9 3JW, UK.

²University of Reading, Reading, UK

³National Centre for Atmospheric
Science-Climate Division, Walker Institute,
University of Reading, Reading, UK.

3 **Abstract.**

4 While changes in land precipitation during the last 50 years have been at-
5 tributed in part to human influences, results vary by season, are affected by
6 data uncertainty and do not account for changes over ocean. One of the more
7 physically robust responses of the water cycle to warming is the expected
8 amplification of existing patterns of precipitation and evaporation. Here, pre-
9 cipitation changes in wet and dry regions are analysed from satellite data
10 for 1988-2010, covering land and ocean. We derive fingerprints for the ex-
11 pected change from climate model simulations that separately track changes
12 in wet and dry regions. The simulations used are driven with anthropogenic
13 and natural forcings combined (ALL), and greenhouse gas forcing or natu-
14 ral forcing only. Results of detection and attribution analysis show the fin-
15 gerprint of combined external forcing is detectable in observations and that
16 this intensification of the water cycle is partly attributable to greenhouse gas
17 forcing.

1. Introduction

18 As temperatures rise in response to increasing greenhouse gas concentrations, the global
19 water cycle is expected to intensify [Allen and Ingram, 2002; Trenberth et al., 2003]. This
20 should lead to increasing atmospheric water vapor and moisture transport, from water
21 exporting to importing regions, enhancing existing patterns of precipitation (P) minus
22 evaporation (E) [Held and Soden, 2006; Seager and Naik, 2012]. Due to energy budget
23 constraints in the atmosphere, the precipitation response in models is 2-3% K⁻¹ [Held
24 and Soden, 2006; Stephens and Ellis, 2008], less than the increase in the water vapour
25 concentrations of ~7% K⁻¹ near to the surface [Santer et al., 2007; Willett et al., 2010].

26 The pattern of wet regions becoming wetter and dry regions becoming drier is seen in
27 multiple satellite based datasets of precipitation [Liu et al., 2012; Chou et al., 2013], in
28 studies of atmospheric moisture transport using reanalysis data [Zahn and Allan, 2011],
29 modeling studies of past and projected changes [Sun et al., 2007; Seager and Naik, 2012;
30 Lau et al., 2013; Liu and Allan, 2013] and changes suggested by ocean salinities [Durack
31 et al., 2012]. It is also consistent with a wider frequency distribution of precipitation
32 [Lintner et al., 2012; Giorgi et al., 2011; Biasutti, 2013].

33 Changes in zonally averaged land precipitation since the 1950s have been partly at-
34 tributed to anthropogenic forcing [Zhang et al., 2007; Polson et al., 2013] using fingerprint
35 detection and attribution (D+A) methods. Changes over the land and ocean combined
36 should show higher signal-to-noise ratio [Balan Sarojini et al., 2012] and the expected
37 change pattern is less clear over land than oceans [Held and Soden, 2006]. Here we apply
38 a D+A analysis [Allen and Stott, 2003] to satellite data for land and ocean precipitation

39 for the years 1988 to 2010. This is a short timescale for analyzing precipitation trends
40 compared to natural variability, however *Seager and Naik* [2012] find anthropogenically
41 induced changes in P-E are beginning to emerge for the satellite period using model and
42 reanalysis data. Our analysis focuses on changes in wet and dry regions separately, relying
43 on expected changes from well understood physical processes and the predicted response
44 to warming. It follows the wet and dry regions as they move over time, tracking the
45 changes in these regions independently of their location [*Liu et al.*, 2012] and thus ac-
46 counting for changes in atmospheric circulation due to natural variability, or in response
47 to warming, for example, poleward migration of the subtropical dry regions [*Seager and*
48 *Naik*, 2012].

49 Climate model simulations of the 20th century are used to derive fingerprints of precip-
50 itation response to all external forcings and greenhouse gas only forcing. Natural forcing
51 can also affect precipitation. Aerosols from volcanic eruptions reduces precipitation par-
52 ticularly in the wet regions for up to 6 years after the eruption in climate models [*Iles*
53 *et al.*, 2013]. The eruptions of El Chichon in 1982 and Pinatubo in 1991 may have im-
54 pacted precipitation during first half of the observation period [*Trenberth and Dai*, 2007],
55 leading to a naturally forced trends that are similar to those due to greenhouse gas forcing.

2. Data: Observations and Models

56 We use the satellite-based Global Precipitation Climatology Project (GPCP) gridded
57 dataset of monthly precipitation [*Adler et al.*, 2003] for the years 1987-2010 (for which
58 measurements from the Special Sensor Microwave Imager (SSM/I) are available). Two
59 observational datasets of monthly land precipitation, the Climate Research Unit (CRU)
60 [*Harris et al.*, 2013] and the Global Precipitation Climatology Centre (GPCC) [*Schneider*

61 *et al.*, 2011] datasets, are included for comparison. ENSO is removed from the observations
62 as the short record means it will influence the trends (note the supplement discusses the
63 robustness of our findings, including to removing ENSO).

64 Model data are from the Climate Model Intercomparison Project Phase 5 (CMIP5)
65 archive [*Taylor et al.*, 2011]. We use historical runs with anthropogenic and natural
66 forcings (ALL), greenhouse gas only forcing (GHG) and natural only forcing (NAT). We
67 also analyze the expected change for 2011-2033, based on the rcp4.5 scenario (Table S1).
68 Data are aggregated to a 5°x5° grid and gridboxes split into land and ocean using the
69 model land fraction data with a cutoff of 50%.

3. Analysis of changes in Wet and Dry Regions

70 Data were divided into zonal bands from 60°-40°S, 40°-20°S, 20°S-0°, 0°-20°N, 20°-
71 40°N and 40°-60°N and then split into wet and dry regions (see below). As satellite
72 observations are less reliable poleward of 50-55° (Huffman pers. comm.), the mid and
73 high latitudes are excluded from the D+A analysis. The data were grouped into four
74 seasons; January, February and March (JFM), April, May June (AMJ), July, August and
75 September (JAS) and October, November and December (OND), to capture the tropical
76 wet and dry seasons, and precipitation averaged across the three months. Precipitation
77 changes are calculated for 1988-2010, to ensure OND and JFM are consistent, OND is
78 from the previous year (1987-2009). Two methods are used to define the dry and wet
79 regions in each zonal band, with all D+A analysis using the precipitation changes from
80 method 1.

81 *Method 1* uses dry and wet regions of fixed size that move from season to season and
82 year to year. For each zonal band, $\hat{P}_x(i, t)$ is the mean precipitation in the dry or wet

83 region for season i and year t where x is *dry* or *wet*. gridboxes are sorted from lowest to
 84 highest precipitation so that

$$\hat{P}_{dry}(i, t) = \sum_{n=1}^{L_{33}} P_n(i, t) \quad (1)$$

85 where P_n is the precipitation in gridbox n and $\hat{P}_{dry}(i, t)$ is the mean precipitation for
 86 all gridboxes in the lower 33.3 percentile ($n \in [1, L_{33}]$), for season i , year t . $\hat{P}_{wet}(i, t)$ is
 87 the mean precipitation of all gridboxes in the upper 33.3 percentile ($n \in [U_{33}, N]$), where
 88 N is the total number of gridboxes in each zonal band. A linear least squares regression
 89 is used to calculate the change in $\hat{P}_x(i, t)$ over all years, $\dot{P}_x(i)$ where $\dot{P}_x(i)$ is expressed
 90 as a percentage relative to $\hat{P}_x(i, t)$ averaged over all years.

91 *Method 2* uses a fixed cutoff value in each zonal band for dry and wet regions for all
 92 years. This allows the regions to move and change size from season to season and year to
 93 year. For each zonal band, $P_{33}(i)$ is the 33.3 percentile for all gridboxes, in all years for
 94 season i and $P_{66}(i)$ is the 66.67 percentile. If $P_n(i, t)$ are sorted from lowest to highest

$$\hat{P}_{dry}(i, t) = \sum_{n=1}^{n_{P33}} P_n(i, t) \quad (2)$$

95 here $n \in [1, n_{P33}]$ are all gridboxes where $P_n(i, t) \leq P_{33}(i)$. For $\hat{P}_{wet}(i, t)$, $n \in [n_{P66}, N]$
 96 are all gridboxes where $P_n(i, t) \geq P_{66}(i)$. $\dot{P}_x(i)$ is then calculated as in method 1.

97 The same methods are applied to individual simulations to calculate $\dot{P}_x(i)$ in each,
 98 these are averaged to give the multi-model mean changes. This allows for differences in
 99 the precipitation patterns and model error in the location of climatological precipitation.

100 Thus the model fingerprints are more physically consistent than that obtained by simply
101 averaging across all simulations which may smear out changes.

4. Detection and Attribution

102 Total least squares regression [Allen and Stott, 2003] determines the magnitude of the
103 fingerprint, \mathbf{F} , of the response to external forcing, in the observations \mathbf{y} .

$$\mathbf{y} = (\mathbf{F} + \varepsilon_{\text{finger}}) \cdot \beta + \varepsilon_{\text{noise}} \quad (3)$$

104 where \mathbf{y} is rank- l vector and \mathbf{F} is a $l \times p$ matrix for p external climate forcings. β
105 is a vector of scaling factors with p entries giving the magnitude of each fingerprint in
106 the observations, $\varepsilon_{\text{noise}}$ is the residual associated with internal climate variability and is
107 compared to samples of model variability using the F-test [Allen and Stott, 2003]. $\varepsilon_{\text{finger}}$
108 is a $l \times p$ matrix of variability superimposed on the fingerprint.

109 Here, single fingerprints ($p = 1$) are used for ALL, GHG, NAT and RCP4.5. In each
110 case \mathbf{F} is the multi-model mean $\dot{P}_x(i)$ for the 4 zonal bands in the tropics and subtropics
111 for seasons $i = 1,4$, giving $l = 16$ for the dry and wet regions separately and $l = 32$ for
112 the dry and wet regions combined. A two-signal approach was applied to GHG and NAT
113 forcing. All analysis was repeated for land+ocean, land only and ocean only. Optimized
114 fingerprints were tried but did not improve the signal-to-noise ratio.

115 Multiple samples of climate noise are added to \mathbf{F} and \mathbf{y} and β recalculated. If $\beta >$
116 0 at the 5% significance level, then the fingerprint response pattern is detected in the
117 observations [Hegerl et al., 2007]. As models may underestimate precipitation variability,
118 β is also calculated for double the model variance [Zhang et al., 2007; Polson et al., 2013].

5. Results

119 The location and size of the GPCP dry and wet regions do not change much from year
120 to year (Figure 1) with 70%-85% of the dry and wet regions remaining fixed from one year
121 to the next. The models tend to locate the dry and wet regions in the same gridboxes as
122 the observations. If the observations define a gridbox as dry(wet) in over 75% of years
123 then on average, 73%(65%) of simulations will also define that gridbox dry(wet) in over
124 75% of years. The size of the regions from the start to the end of the observation period
125 change by less than the maximum year-to-year variation, except in SH mid-latitudes.

126 The tropics and subtropics show a pattern of dry regions becoming drier and wet regions
127 becoming wetter from 1988-2010 for the observations and multi-model means for models
128 with greenhouse gas forcing (ALL, GHG, RCP4.5, see Figure 2). The NAT only multi-
129 model mean also shows a tendency for dry to get drier and wet to get wetter, but not as
130 consistently for all zonal bands and seasons. However, these patterns are not consistent
131 across all simulations. 20-30% of the ALL, GHG and RCP4.5, and 40% of the NAT
132 only individual simulations give more (i.e zonal bands and seasons) dry regions becoming
133 wetter. Wet regions becoming wetter is a more consistent result with exceptions of less
134 than 10% of the ALL forced and GHG only simulations and <20% of the RCP4.5 and
135 NAT forced simulations. While the pattern of moistening and drying persists over both
136 land and ocean in observations and models (Figures S13 and S14), dry becoming drier is
137 more consistent over oceans than land. Comparison of the GPCP land only changes with
138 two other station-based observational datasets, GPCC and CRU (masked to the wet and
139 dry regions of GPCP), shows consistency between the datasets (Figures S15 and S16).

140 The detection analysis for the combined fingerprint of the wet and dry regions and all
141 seasons combined shows that ALL forcing had a significant influence on satellite measure-
142 ments of precipitation (Figure 3(a)). The changes from GHG and RCP4.5 simulations
143 are similarly detected in the observed changes, while NAT forcing is not (Figure S17).
144 Changes are also detected over ocean only, but not land only, likely due to poorer signal-
145 to-noise ratio with a smaller fraction of the wet and dry regions coinciding with land than
146 ocean and a quicker response to more localized forcing (see *Balan Sarojini et al.* [2012]).
147 SH tropical dry regions in OND and JFM, and SH subtropical wet regions in AMJ and
148 JAS were excluded from the land only analysis because few gridboxes coincide with land.

149 Changes in the dry and wet regions separately are also detected for ALL, GHG and
150 RCP4.5 forcing, (over ocean for ALL forcing, Figure S19). The fingerprint of NAT forcing
151 is also detectable for the wet regions, possibly reflecting the influence of volcanoes during
152 the first half of the observation period [*Iles et al.*, 2013]. To distinguish the influence of
153 GHG from NAT forcing, a 2-signal D+A was applied, simultaneously estimating GHG
154 and NAT forcing. The results for the combined dry and wet fingerprint shows that GHG
155 forcing is detectable while NAT forcing is not (Figure 3(b)).

156 Our results were robust to not removing ENSO and using the Nino-3.4 SST index from
157 CPC, NOAA (see supplement), except when ENSO is not removed, ALL forcing for the
158 dry+wet fingerprint was not detected for land+ocean, while GHG forcing was detectable
159 in the dry regions for the GHG and NAT 2-signal analysis.

6. Discussion and Conclusions

160 Precipitation from GPCP observations and models that include GHG forcing (i.e. ALL,
161 GHG only and RCP4.5) clearly show a tendency for dry regions to get drier and wet regions

162 to get wetter, consistent with theory [*Allen and Ingram, 2002; Held and Soden, 2006*]. The
163 NAT only simulations show a similar pattern for the wet regions and to a lesser extent
164 in the dry regions due to the influence of the El Chichon and Pinatubu eruptions in the
165 first half of the observation period.

166 The zonal mean changes for the GPCP data are dominated by changes over the ocean
167 which are thought to be less reliable than changes over land (e.g. *Liu et al. [2012]*).
168 While the pattern of wet regions becoming wetter holds over both land and ocean, drying
169 in the dry regions is less consistent over land. There is evidence that land and ocean
170 precipitation are anti-correlated [*Liu et al., 2012*], however, on short timescale, this is due
171 to the influence of ENSO, hence we lose much of this anti-correlation here.

172 Detection and attribution analysis shows all external forcings and greenhouse forcing are
173 detectable in precipitation changes over the last 20 years in the tropical and subtropical
174 dry and wet regions. Fingerprints based on future change are also detectable showing
175 they are expected to enhance the pattern of change already observed.

176 If the wet and dry signals are combined, greenhouse gas forcing can be detected sep-
177 arately to natural forcing. The precipitation response to volcanic eruptions in the dry
178 regions is small compared to the greenhouse gas signal, which may explain why the green-
179 house gas signal is detectable in the dry regions while the natural signal is not in the
180 1-signal analysis. Our analysis did not include aerosol changes explicitly as not enough
181 runs were available to characterize changes with reasonable signal-to-noise ratio.

182 Our results are subject to uncertainty in trends derived from satellite data and the
183 shortness of the observational record. However, our results are consistent with results
184 attributing salinity changes to human influences [*Durack et al., 2012*] over ocean, and

185 changes recorded over land are broadly similar to those recorded by in-situ data. Thus
186 our results suggest an emerging pattern of wet regions becoming wetter and dry regions
187 becoming drier that appears to be at least in part due to greenhouse gas forcing. This
188 provides evidence of an anthropogenically-induced intensification of the water cycle.

189 **Acknowledgments.** We acknowledge the Global Precipitation Climatology Project,
190 the Global Precipitation Climatology Centre and the Climatic Research Unit. We thank
191 the World Climate Research Programme’s Working Group on Coupled Modelling, the
192 climate modeling groups (Table S1), the U.S. Department of Energy’s Program for Climate
193 Model Diagnosis and Intercomparison, the Global Organization for Earth System Science
194 Portals and the anonymous reviewers. This work was supported by the NERC project
195 PAGODA (NE/I006672/1), the National Science Foundation (ATM-0296007), NCAS, the
196 US Department of Energy’s Office of Science and NOAA’s Climate Program Office.

References

- 197 Adler, R., et al. (2003), The version 2 global precipitation climatology project (gpcp)
198 monthly precipitation analysis (1979-present), *J. Hydrometeor.*, *4*, 1147–1167.
- 199 Allen, M., and W. Ingram (2002), Constraints on future changes in climate and the
200 hydrologic cycle, *Nature*, *419*(6903), 224–232.
- 201 Allen, M., and P. Stott (2003), Estimating signal amplitudes in optimal fingerprinting,
202 Part I: Theory, *Clim. Dyn.*, *21*(5), 477–491.
- 203 Balan Sarojini, B., P. A. Stott, E. Black, and D. Polson (2012), Fingerprints of changes
204 in annual and seasonal precipitation from cmip5 models over land and ocean, *Geophys.*
205 *Res. Lett.*, *39*(21), L21,706, doi:10.1029/2012GL053373.

206 Biasutti, M. (2013), Climate change: Future rise in rain inequality, *Nature Geosci.*, 6(5),
207 337–338.

208 Chou, C., J. C. H. Chiang, C.-W. Lan, C.-H. Chung, Y.-C. Liao, and C.-J. Lee (2013),
209 Increase in the range between wet and dry season precipitation, *Nature Geosci.*, 6(4),
210 263–267.

211 Durack, P. J., S. E. Wijffels, and R. J. Matear (2012), Ocean salinities reveal strong global
212 water cycle intensification during 1950 to 2000, *Science*, 336(6080), 455–458.

213 Giorgi, F., et al. (2011) Higher Hydroclimatic Intensity with Global Warming, *J. Clim.*,
214 24(20), 5309–5324.

215 Harris, I., P. Jones, T. Osborn, and D. Lister (2013), Updated high-resolution grids of
216 monthly climatic observations – the cru ts3.10 dataset, *Int. J. Climatology*, *accepted*.

217 Hegerl, G. C., et al. (2007) Detection of human influence on a new, validated 1500-year
218 temperature reconstruction, *J. Clim.*, 20(4), 650–666.

219 Held, I., and B. Soden (2006), Robust Responses of the Hydrological Cycle to Global
220 Warming, *J. Clim.*, 19(21), 5686–5699.

221 Iles, C. E., G. C. Hegerl, A. C. Schurer, and X. Zhang (2013), The effect of volcanic
222 eruptions on global precipitation, *J. Geophys. Res: Atmospheres*, *accepted*.

223 Lau, W. K.-M., H.-T. Wu, and K.-M. Kim (2013), A canonical response of precip-
224 itation characteristics to global warming from cmip5 models, *Geophys. Res. Lett.*,
225 doi10.1002/grl.50420.

226 Lintner, B. R., et al. (2012), Amplification of wet and dry month occurrence over tropical
227 land regions in response to global warming, *J. Geophys. Res: Atmospheres*, 117, doi:
228 10.1029/2012JD017499.

229 Liu, C., R. P. Allan, and G. J. Huffman (2012), Co-variation of temperature and precipi-
230 tation in cmip5 models and satellite observations, *Geophys. Res. Lett.*, *39*(13), L13,803,
231 doi:10.1029/2012GL052093.

232 Liu, C., and R. P. Allan (2013), Observed and simulated precipitation responses in
233 wet and dry regions 1850-2100., *Environ. Res. Lett.*, *8*, 034002, doi:0.1088/1748-
234 9326/8/3/034002.

235 Polson, D., G. C. Hegerl, X. Zhang, and T. J. Osborn (2013), Causes of robust seasonal
236 land precipitation changes, *J. Clim.*, doi:10.1175/JCLI-D-12-00474.1.

237 Santer, B., et al. (2007), Identification of human-induced changes in atmospheric moisture
238 content, *Proc. Natl. Acad. Sci. USA*, *104*, 15,244–15,253.

239 Schneider, U., A. Becker, A. Meyer-Christoffer, M. Ziese, and B. Rudolf (2011), Global
240 precipitation analysis products of the gpcc, [http://gpcc.dwd.de/](http://gpcc.dwd.de/below) below "Publications".

241 Seager, R., and N. Naik (2012), A mechanisms-based approach to detecting recent an-
242 thropogenic hydroclimate change, *J. Clim.*, *25*, 236–261.

243 Stephens, G. L., and T. D. Ellis (2008), Controls of global-mean precipitation increases
244 in global warming gcm experiments, *J. Clim.*, *21*(23), 6141–6155.

245 Sun, Y., S. Solomon, A. Dai, and R. W. Portmann (2007), How often will it rain?, *J.*
246 *Clim.*, *20*(19), 4801–4818.

247 Taylor, K. E., R. J. Stouffer, and G. A. Meehl (2011), An overview of cmip5 and the
248 experiment design, *Bull. Amer. Meteor. Soc.*, *93*(4), 485–498.

249 Trenberth, K. E., A. Dai, R. Rasmussen, and D. Parsons (2003), The changing character
250 of precipitation, *Bull. Amer. Meteor. Soc.*, *84*(9), 1205–1217.

251 Trenberth, K. E., and A. Dai (2007), Effects of Mount Pinatubo volcanic eruption on
252 the hydrological cycle as an analog of geoengineering, *Geophys. Res. Lett.*, *34*(15), doi:
253 10.1029/2007GL030524.

254 Willett, K. M., P. D. Jones, P. W. Thorne, and N. P. Gillett (2010), A comparison of large
255 scale changes in surface humidity over land in observations and cmip3 gcms, *Environ.*
256 *Res. Lett.*, *5*, 025,210, doi:10.1088/1748-9326/5/2/025210.

257 Zahn, M., and R. P. Allan (2011), Changes in water vapor transports of the ascending
258 branch of the tropical circulation, *J. Geophys. Res: Atmospheres*, *116*(D18), D18,111,
259 doi:10.1029/2011JD016206.

260 Zhang, X., et al. (2007), Detection of human influence on twentieth-century precipitation
261 trends, *Nature*, *448*(7152), 461–465.

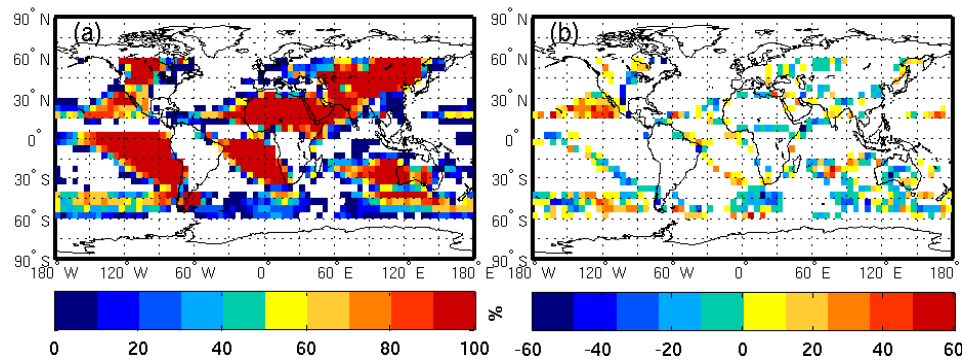


Figure 1. GPCP dry regions for October, November and December (OND is 1987-2009) from method 1. (a) The percentage of years a gridbox is defined as dry for 1987-2009. (b) Percentage of years dry in 2000-2009 minus 1987-1996, only gridboxes where the change is not zero are plotted. ENSO removed from observations. Similar results for other seasons (see supplement).

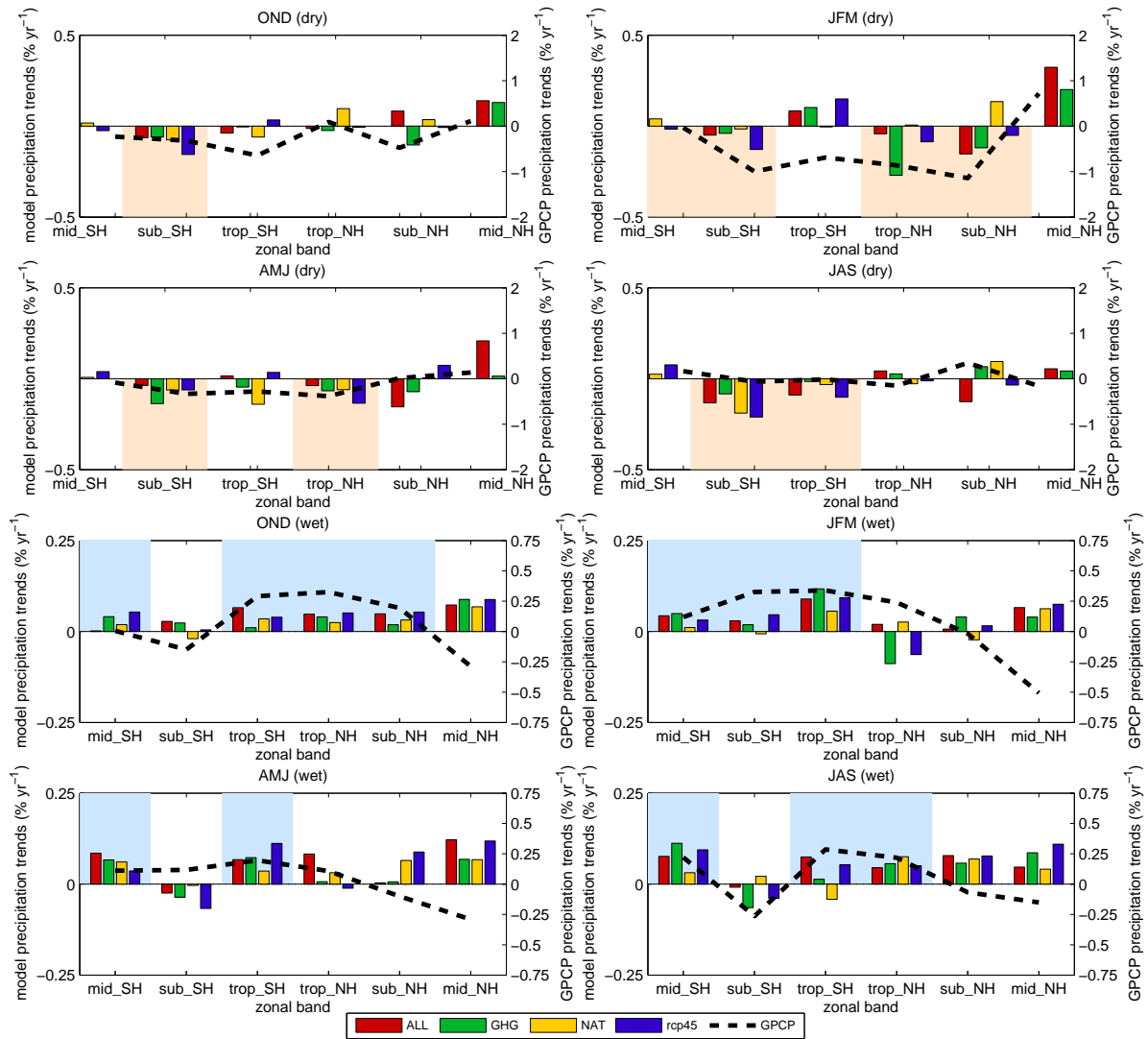


Figure 2. Observed and model simulated zonal mean changes (% per year) in the dry (TOP FOUR PANELS) and wet (LOWER FOUR PANELS) regions for land and ocean 1988 to 2010 (OND is 1987-2009). The colored bars give the multi-model mean changes for the ALL, GHG, NAT and RCP4.5 simulations. The orange/blue shading show where GPCP, ALL and RCP4.5 are all negative/positive. Note GPCP is plotted on a larger scale and the influence of ENSO is removed from observations.

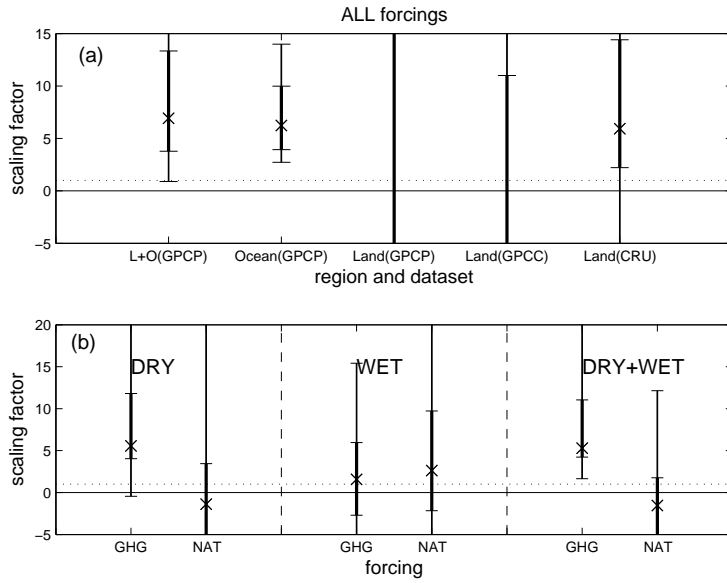


Figure 3. (a) Scaling factors for the wet and dry regions combined for ALL forced simulations. L+O is land+ocean. (b) Scaling factor for 2-signal D+A of GHG and NAT forcing. Crosses show the 'best-guess' scaling factor for the multi-model mean, thick lines are the 90% confidence interval for the raw model variance added as noise and thin lines are the 90% confidence interval for double the variance. Influence of ENSO is removed from observations. The residual consistency test is passed in all cases.